Quantum Dot Spontaneous Emission Lifetime Modification in Optical Microcavities using Oxide Apertured Micropillars

N. G. Stoltz, M. Rakher, S. Strauf, D. Bouwmeester, P. M. Petroff, and L. A. Coldren.
University of California, Santa Barbara, CA 93106.

ABSTRACT

An oxide aperture is used to confine optical modes in a micropillar structure. This method overcomes the limitations due to sidewall scattering loss typical in semiconductor etched micropillars. High cavity quality factors (Q) up to 48 000 are determined by external Fabry-Perot cavity scanning measurements, a significantly higher value than prior work in III-V etched micropillars. Measured Q values and estimated mode volumes correspond to a maximum Purcell factor figure of merit value of 72. A Purcell Factor of 2.5 is experimentally observed from a single quantum dot emitter coupled to a high Q cavity mode.

Keywords: Micropillars, Microcavities, Quantum Dots, Purcell Effect, Quantum Dot-Microcavity Coupling, Time Correlated Photon Counting.

1. INTRODUCTION

Optical microcavities combined with active emitters provide a great opportunity to study the light-matter interaction at a fundamental level. To produce a high quality microcavity it is necessary to confine light to precise resonance frequencies with little or no optical loss [1]. The measure of this optical confinement is referred to as the cavity quality factor (Q). In order to increase the coupling between an emitter and mode in a cavity it is also important to reduce the effective optical mode volume (V_{eff}). When an optical emitter is both spatially and spectrally coupled to a high quality microcavity, the Purcell Effect is observed [2]. The Purcell Effect is experimentally observed through the modification of active emitter spontaneous emission lifetimes. In the weak coupling regime, the spontaneous emission lifetime of an emitter coupled to a microcavity is decreased by the Purcell Factor [2]. The Purcell Factor is proportional to the ratio of Q/V_{eff} and includes factors accounting for both spatial and spectral detuning of the emitter with respect to the cavity. Potential applications include solid state quantum electrodynamics (CQED) experiments, modification of single emitter lifetimes, and single photon emitters and detectors for quantum cryptography [1, 2].

1.1 III-V Semiconductor Microcavity Architectures

Several solid-state microcavity architectures including microdisks [3, 4], photonic crystals [5, 6, 7], and micropillars [8, 9] have shown CQED effects in III-V micropillars using self-assembled quantum dots (QD's) as active emitters. The Purcell Effect has been experimentally observed in each of these microcavity architectures. Microdisks have shown coupled QD lifetimes of 370 ps corresponding to a Purcell Factor of 3.5 [3]. Photonic crystals and micropillars have both shown QD lifetimes of 200 ps corresponding to a Purcell Factor of 5 [6, 8]. In addition all three architectures have exhibited the transition from the weak to strong coupling regime [4, 7, and 9].

Among these architectures, micropillars couple light normal to the semiconductor in a single lobed Gaussian pattern that is easily fiber coupled [10]. This high photon collection efficiency makes micropillars a better alternative for device applications. However, micropillars exhibit higher V_{eff} ($\sim 5\ (\lambda/n)^3$) and lower Q's (~2000-10 000) when compared with photonic crystals [1, 9]. These V_{eff} can be reduced by decreasing pillar diameter, but scattering losses due to sidewall roughness have been shown to limit achievable Q values [1, 11].

1.2 Oxide Aperture Micropillars

An alternative approach using oxide apertured micropillars to reduce V_{eff} while maintaining high Q values has been previously shown [12]. Oxidized micropillars have been used for vertical cavity laser (VCL) applications to produce low threshold laser devices that are fabricated into inexpensive arrays for optical data networks [13]. By confining the

Laser Beam Control and Applications, edited by Alexis V. Kudryashov, Alan H. Paxton, Vladimir S. Ilchenko, Adolf Giesen, Detlef Nickel, Steven J. Davis, Michael C. Heaven, J. Thomas Schriempf,
Proc. of SPIE Vol. 6101, 61010W, (2006) · 0277-786X/06/$15 · doi: 10.1117/12.669580

optical mode with a laterally oxidized aperture layer these structures simultaneously provide optical mode and electrical current confinement while eliminating the scattering loss due to sidewall roughness inherent to etched pillar structures.

This method has been applied to the field of QD-microcavity coupling with limited success due to very low Q's (<1000) as well as high V_{eff} (~35 $(\lambda/n)^3$) when compared with conventional micropillars [14, 15]. Oxidized micropillars have shown QD lifetimes of 900 ns corresponding to a Purcell factor of 2 [14]. If these values are improved, the advantages in ease of fabrication will make oxide apertured micropillars very attractive for coupled QD-microcavity device applications.

2. SAMPLE DESIGN AND FABRICATION

Micropillar samples investigated in this study were grown by molecular beam epitaxy on a semi-insulating GaAs (100) substrate with a 0.1 μm buffer layer. There are four independent sections in the structure: the bottom mirror, the active region, the aperture region, and the top mirror as shown schematically in Fig. 1(a). Mirrors consist of alternating one quarter optical thickness distributed Bragg reflector (DBR) layers of GaAs and $Al_{0.9}Ga_{0.1}As$. 32 pairs of $Al_{0.9}Ga_{0.1}As$/GaAs layers with thicknesses of 79.8/68.4 nm respectively form the bottom DBR mirror, while the top DBR mirror is made of 23 pairs. The active region is one optical wavelength in thickness, with two 135.4 nm layers of GaAs embedding a centered InGaAs/GaAs QD layer. QD's self-assemble during epitaxy operating in the Stranski-Krastanov growth mode. InGaAs islands are partially covered with GaAs and annealed before completely capped with GaAs. This procedure blue shifts the QD's emission wavelengths toward the spectral region where Si-based detectors are more efficient [16]. The thickness of the aperture region is three quarters optical wavelength and consists of a pure AlAs layer sandwiched by $Al_{0.89}Ga_{0.11}As$ and $Al_{0.75}Ga_{0.25}As$ in order to produce the desired oxide aperture qualities. It is designed to give a change in effective index, Δneff = 0.08, between the fully oxidized and unoxidized regions of the micropillar in addition to a linear oxide taper with a length of 1.1 μm after an approximate 10 μm oxidation.

A scanning electron microscopy (SEM) image of a fabricated oxide apertured microcavity is shown in Fig. 1(b), while Fig. 1(c) shows a cross-sectional SEM image of an oxidized mesa calibration sample with mirror, active, and aperture regions corresponding to Fig. 1(a). Samples are fabricated by optical lithography and reactive ion etch (RIE) in Cl_2 plasma penetrating approximately 5 mirror periods into the bottom DBR. Micropillars are fabricated in large arrays with diameters varying from 21-25 μm. The wet lateral oxidation is performed at 430˚C in order to oxidize the aperture region by converting AlAs into Al_xO_y.

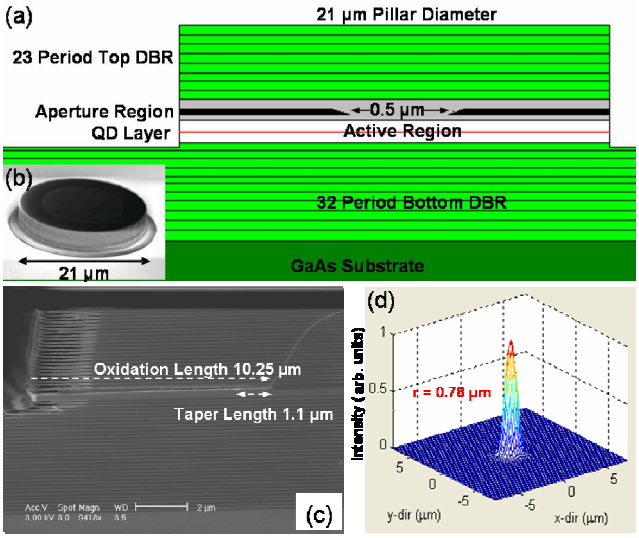

Figure 1 (a) Schematic and layer structure for the oxide apertured micropillars in this study. (b) SEM image of a fully processed 21 μm micropillar. (c) SEM cross-section image of an oxidized mesa calibration showing actual layer structure depicted in (a). (d) The theoretical fundamental mode profile for the 21 μm micropillar modeled in this study with a Gaussian mode radius of 0.78 μm.

3. EXPERIMENTAL SETUP

Micro-photoluminescence (μ-PL) measurements are performed using a He-flow cryostat (4-300K). QD's are excited non-resonantly by a continuous wave 780 nm laser diode focused to a spot size of 2.5 μm using a microscope objective with numerical aperture of 0.55. μ-PL emission is collected through the same objective and recorded with a 1.25 m spectrometer equipped with a charge-coupled device with 30 μeV spectral resolution at 900 nm.

A scanning Fabry-Perot cavity along with a single photon counting avalanche photodiode detector and an integrated counting unit are used to experimentally determine linewidths beyond the resolution of the spectrometer.

Lifetime traces of single QDs are taken by time-correlated photon counting (TCPC) using a Ti:Sa laser operated at 780 nm with a repetition rate of 82Mhz for excitation and a single photon counting avalanche diode for detection. Second order coherence functions are measured by passing the signal through two single photon counting avalanche photodiodes in a Hanbury-Brown and Twiss setup. Measuring the difference in arrival time between photons at each of the two detectors provides a measure of the second order correlation function [17].

Table I.

21μm Pillar Fundamental Mode	
Modeling Parameters	
n_{core}	3.12
Δn	0.081
Core Width (μm)	0.5
Taper Length (μm)	1.1

Simulation Results	
L_{eff} (μm)	1.39
α_{rad} (cm^{-1})	1.66e-3
α_{scat} (cm^{-1})	1.66
α_m (cm^{-1})	13.86
Γg_{th} (cm^{-1})	14.69
λ (nm)	914.36
Q_{cold}	14 480
$V_{eff}[(\lambda/\mathrm{n})]^{-3}$	51
Γ	3.65e-3

Experimental Results	
λ (nm)	914.11
$Q_{\exp}$	48 000
F_p	72
$\Gamma g_{\exp}$ (cm^{-1})	10.44

Table I. Simulation parameters, theoretical results, and experimental values are given for the fundamental mode of the 21 μm diameter micropillar in this study.

4. MODELING THE CAVITY

A two-dimensional model of the cavity has been developed based on the experimentally determined values for the oxide aperture taper length and core width from SEM images (Fig. 1) along with the one-dimensional reflectivity spectrum of the unprocessed sample. This produces a two-dimensional index profile determined by the effective index (n_{eff}) in the growth direction for the unoxidized and oxidized layer stack. The Δn_{eff} between the unoxidized and oxidized regions is evaluated by replacing the AlAs and $Al_{0.89}G\ a_{0.11}As$ with Al_xO_y (n=1.5). It has been demonstrated [18] that the linear oxide taper shown in Fig. 1(c) corresponds to a parabolic index grade over the length of the taper.

We used this model to solve for the eigenmodes of the two-dimensional scalar wave equation using a finite difference technique with a non-uniform mesh [19]. The solution for the fundamental mode of a 21μm pillar (with parameters given in Table 1) is shown in Fig. 1(d) and has a Gaussian mode radius of approximately 0.78 μm. Scattering and radiation losses are determined by propagating a scalar field around the unfolded cavity until the field no longer changes shape. This procedure is analogous to the classic work of Fox and Li [20].

Mirror, scattering, and radiation losses determine the empty or cold cavity linewidth of the apertured micropillar. Assuming that undoped AlGaAs regions have no internal optical loss at 4K, the only optical loss mechanisms in the cavity are due to mirror loss (α_m), radiation loss (α_{rad}), and aperture scattering losses (α_{scat}) [19]. Furthermore, α_{rad} and α_{scat} are very small for the fundamental mode, 1.66e-3 and 1.66 cm^{-1} respectively. This leaves photon escape through the top DBR mirror as the dominating loss mechanism in the cavity; here α_m is calculated as 13.86 cm^{-1}. Cold cavity (Q_{cold}) values are determined by these cavity losses according to $\frac{\omega}{Q_{cold}} = \frac{1}{\tau_p} = v_g \Gamma g_{th} = v_g (\alpha_{scat} + \alpha_{rad} + \alpha_m)$ [19]. Here τ_p is cavity lifetime, v_g is group velocity, ω is frequency, Γ is the confinement factor, and g_{th} is the threshold material gain. The estimated Q_{cold} for a 21 μm micropillar is 14 480. Other theoretical values for various parameters are given in Table 1 for a 21μm micropillar.

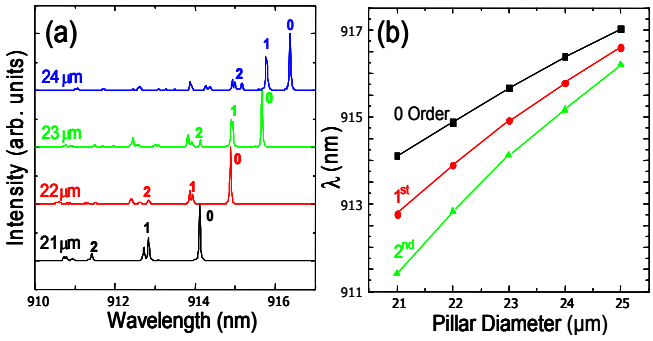

Figure 2 (a) Normalized optical mode spectra for 21-25 um micropillars measured by μ-PL at 4 K are shown. Fundamental, first, and second order modes are labeled by numbers 0, 1, and 2 respectively. (b) Mode position in nm is shown as a function of pillar diameter for fundamental, first, and second order modes.

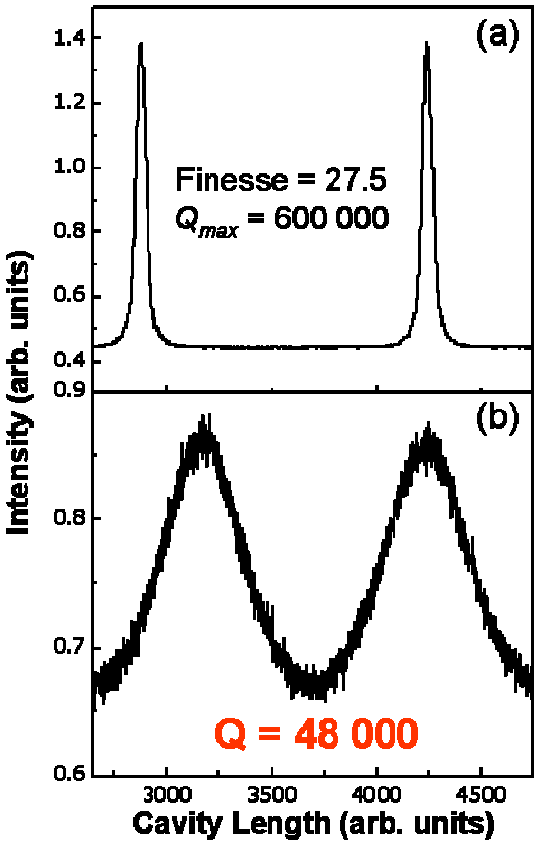

Figure 3 (a) Transmission through a Fabry-Perot cavity as a function of cavity length for a reference laser. Using the given free spectral range of the measurement cavity, the reference laser has Q > 600000 giving a maximum measurable Q. (b) The Fabry-Perot measurement of the fundamental mode linewidth of a 21 μm micropillar cavity. The measured linewidth corresponds to Q > 48000. This measurement was done at 50 μW pump power at 4 K.

5. EXPERIMENTAL MODE SPECTRA

Experimental mode spectra for 21-25μm diameter pillars are shown in Fig. 2(a). Mode orders 0, 1, and 2 are labeled in Fig. 2(a). The lifting of higher order mode degeneracy is due to asymmetry in the fabrication process. μ-PL data shows cavity modes with lower fundamental energies as well as increasing mode spacing as pillar diameter decreases. This effect is shown in Figure 2(b) for varying pillar diameters. In addition, intensity decreases are observed for higher order modes due to increased scattering losses, an intentional effect produced by the oxide aperture and the larger effective radii of multi-lobed higher order modes.

A Fabry-Perot scanning cavity is used to determine experimental Q values. First a reference laser is used to calibrate the maximum measurable Q for the Fabry-Perot cavity as 600 000, shown in Fig. 3(a). The fundamental cavity mode is then directed through a 1 nm bandpass filter into the detector for sample measurement. Experimental quality factor (Q_{exp}) is determined to be approximately 48 000 for a 21 μm pillar as shown in Fig. 3(b). This value is larger than the theoretical cold cavity value due to linewidth narrowing caused by modal gain from the QD active region. The gain in the QD active region (g_{exp}) is determined by the relationship between Q_{cold} and Q_{exp} values according to

$$\frac{\omega}{Q_{\exp}} = \frac{\omega}{Q_{cold}} - v_g \Gamma g_{\exp}$$ [19]. Estimated gain values are shown in Table I.

Q values show little change with increasing pump power and no laser threshold behavior is observed up to 50 μW pump power. This indicates that material gain in the QD layer saturates before the threshold condition is achieved. Estimated values show that g_{exp} in the QD active region saturates at approximately 10.44 cm^{-1}, corresponding to approximately 2864 cm^{-1} material gain from the active region. This is a reasonable value for the single QD layer in this cavity design [21].

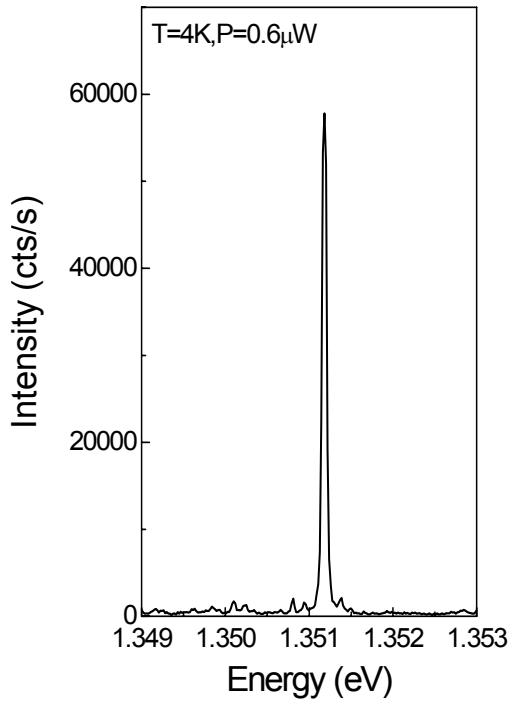

Figure 4. Optical spectra of device G7 taken at low pump powers of 600 nW at 4K. The spectra shows sharp resolution limited transition lines.

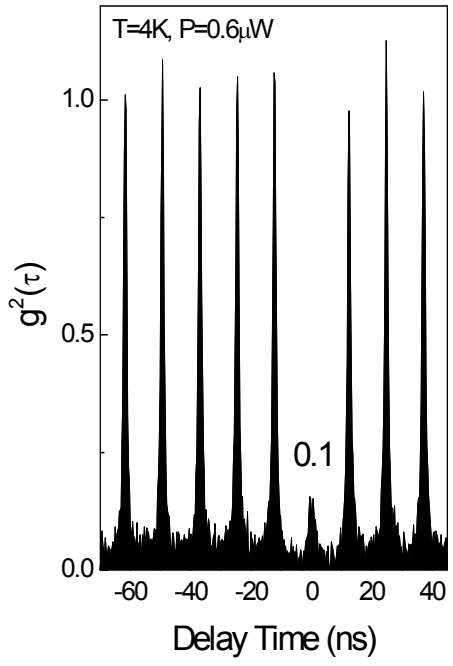

Figure 5. Second order coherence as a function of delay time for device G7 showing pronounced photon antibunching. The zero delay time peak area is ~10 % with respect to the sidepeak areas. This is indicative of a single photon emitter.

6. EXPERIMENTAL OBSERVATION OF THE PURCELL EFFECT

The Purcell factor determines the figure of merit for a coupled QD-microcavity in the weak coupling regime. Using theoretical V_{eff} and experimental Q_{exp} values it is possible to estimate the maximum achievable F_p according to $F_p = \frac{3}{4\pi^2}\frac{Q\left(\lambda/n_{eff}\right)^3}{V_{eff}}$ [22]. Experimentally observed values are decreased due to spectral and spatial detuning. Estimating the Purcell factor with experimental linewidths gives a maximum value of 72.

The experimental spectra for a QD coupled to a fundamental cavity mode for 21 μm oxidized micropillar device G7 is shown in Fig. 4. This device exhibits sharp resolution limited modes at approximately 1.351 eV under low excitation powers of 0.6 μW. The second order coherence function shows that this spectrum is due to single QD emission as shown in Fig. 5. Multiple non-interacting QD emitters show a zero delay time peak ≥ 0.5, while single QD emitters show a zero delay time peak ≤ 0.5. Here the zero delay time peak is approximately 10% with respect to the sidepeaks. This corresponds to a 10 times decrease in multiphoton emission events if compared to an attenuated laser (Poissonian) light source and is indicative of a single photon source.

TCPC lifetime traces of this device are shown in Fig. 5. QD spontaneous emission lifetimes of 440 ps are observed. A reference QD lifetime from a sample without a cavity exhibits spontaneous emission lifetimes of 1100 ps. This corresponds to a Purcell factor of approximately 2.5 when compared to the reference QD. Maximum achievable Purcell effects are limited due to the random spatial position of the QDs with respect to the cavity mode.

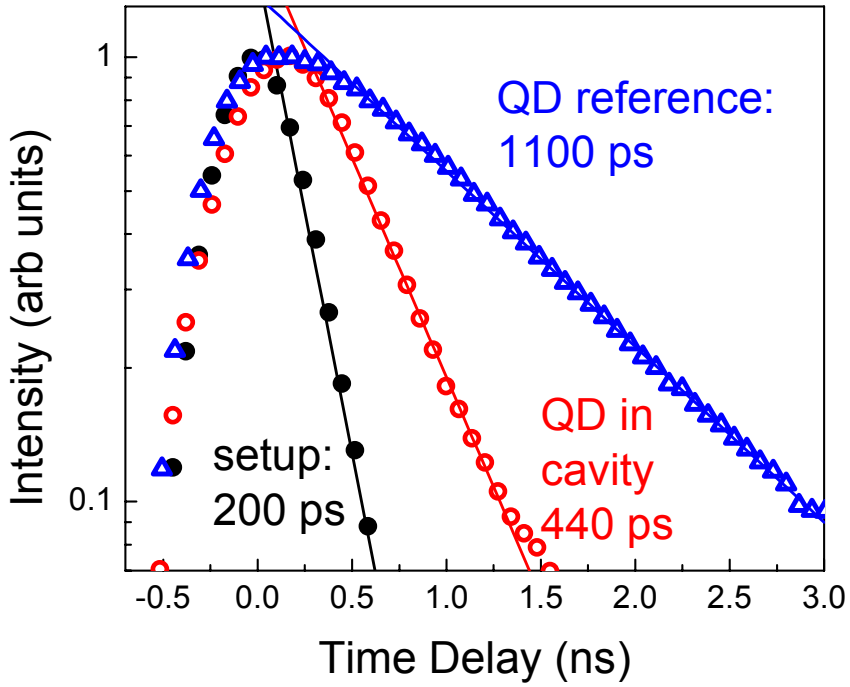

Figure 6. Lifetime traces of single QDs taken by time-correlated photon counting (TCPC) using a Ti:Sa laser operated at 780 nm with a repetition rate of 82Mhz for excitation and a single photon counting avalanche diode for detection. Data have been taken for a reference sample without a cavity (open blue triangles) and for a typical single QD spectrally tuned into resonance with a micropillar cavity mode (open red circles). The black circles are the system response for a short laser pulse illustrating the timing resolution of the setup of 200 ps.

7. CONCLUSIONS

Oxidized micropillars have a promising outlook for QD-microcavity coupling due to high Q values. Further improvement for these devices could be achieved by reducing V_{eff}. Although oxide aperture micropillars reduce two dimensional mode areas while maintaining high Q values, V_{eff} remains relatively high. This is due to the large effective cavity length (L_{eff}) in the growth direction of this structure, approximately 1.39 μm. Improvement lies in reducing this L_{eff} value, potentially by replacing AlGaAs/GaAs DBR mirrors with Al_xO_y/GaAs DBR mirrors having reduced mirror penetration depths.

The observed Purcell factor of 2.5 is smaller that the theoretical maximum value of 72. This is due to spatial detuning of the QD emitter with respect to the cavity mode. Micropillars are fabricated on a random array of quantum dots. When the QD emitter is not spatially aligned to an electric field maximum of the cavity mode a corresponding decrease in the Purcell Effect occurs. This spatial detuning may potentially be overcome by developing active positioning schemes that fabricate pillars around known QD candidates.

Experimental data shows very high Q (48 000) optical microcavities using an oxide apertured micropillar architecture. Devices exhibit controlled mode positions and sizes down to core widths of approximately 0.5 μm. Unlike etched air interface micropillars, which can be difficult to fabricate with acceptable loss values at smaller diameters, apertured micropillars accomplish this in a controllable and repeatable fashion. Cavities exhibit low loss values resulting from gain related linewidth narrowing effects due to stimulated emission from the QD active region. Apertured micropillars show promise for QD-microcavity coupling applications due to these high experimental Q values producing a maximum Purcell factor of 72. A Purcell Factor of approximately 2.5 is experimentally observed in a single QD emitter coupled to a cavity mode.

REFERENCES

[1] J. M. Gerard, in *Single Quantum Dots: Fundamentals, Applications, and New Concepts*, edited by P. Michler (Springer, Berlin, 2003), Vol. **90**, Chap. 4, p.269-314.

[2] K. J. Vahala, Nature **424**, 839 (2003).

[3] A. Kiraz, P. Michler, C. Becher, B. Gayral, A. Imamoglu, L. Zhang, W. V. Schoenfeld, and P. M. Petroff, Appl. Phys. Lett. **78**, 3932 (2001).

[4] E. Peter, P. Senellart, D. Martou, A. Lemaitre, J. Bloch, J. Hours, and J. M. Gerrard, in preparation (available at http://xxx.lanl.gov/abs/quant-ph/0411076).

[5] T. D. Happ, I. I. Tartakovski, V. D. Kulakovskii, J. –P. Reithmaier, M. Kamp, and A. Forchel, Phys. Rev. B **66**, 041303 (2002).

[6] A. Badolato, K. Hennessy, M. Atature, J. Dreiser, E. Hu, P. M. Petroff, and A. Imamoglue, Science **308**, 1158 (2005).

[7] T. Yoshie, A. Scherer, J. Hendrickson, G. Khitrova, H. M. Gibbs, G. Rupper, C. Ell, O. B. Shchekin, and D. G. Deppe, Nature **432**, 200 (2004).

[8] J. Vuckovic, D. Fattal, C. Santori, G. S. Solomon, and Y. Yamamoto, Appl. Phys. Lett. **82**, 3596 (2003).

[9] J. P. Reithmaier, G. Sek, A. Loffler, C. Hormann, S. Kuhn, S. Reitzenstein, L. V. Keldysh, V. D. Kulakovski, T. L. Reinecke, and A. Forchel, Nature **432**, 197 (2004).

[10] M. Pelton, J. Vukovic, G. S. Solomon, A. Scherer, and Y. Yamamoto, IEEE J. Quantum Electron. **38**, 170 (2002).

[11] T. Rivera, J. –P. Debray, J. M. Gerard, B. Legrand, L. Manin-Ferlazzo, and J. L. Oudar, Appl. Phys. Lett. **74**, 911 (1999).

[12] N. G. Stoltz, M. Rakher, S. Strauf, A. Badolato, D. Lofgreen, P. M. Petroff, L. A. Coldren, and D. Bouwmeester, Appl. Phys. Lett. **87**, 031105 (2005).

[13] L. A. Coldren, H. Temkin, and C. W. Wilmsen, *Vertical-Cavity Surface-Emitting Laser*, **First** edition (Cambridge University Press, Cambridge, UK, 1999), Vol. **1**, Chap. 1, p.1.

[14] L. A. Graham, D. L. Huffaker, and D. G. Deppe, Appl. Phys. Lett. **74**, 2408 (1999).

[15] D. G. Deppe, L. A. Graham, and D. L. Huffaker, IEEE J. Quantum Electron. **35**, 1502 (1999).

[16] P. M. Petroff, A. Lorke, and A. Imamoglu, Physics Today **54**, 46 (2001).

[17] B. D. Gerardot, S. Strauf, M. J. A. de Dood, A. M. Bychkov, A. Badolato, K. Hennessy, E. L. Hu, D. Bouwmeester, and P. M. Petroff, Phys. Rev. Lett. **95**, 137403 (2005).

[18] E. R. Hegblom, N. M. Margalit, A. Fiore, and L. A. Coldren, IEEE J. Sel. Top. Quantum Electron. **5**, 553 (1999).

[19] Larry A. Coldren and Scott W. Corzine, in *Diode Lasers and Photonic Integrated Circuits*, **First** edition, edited by Kai Chang (John Wiley & Sons, INC., New York, 1995), Vol. **1**, Ch. 16 Apps. 4,16, pp. 188,226,444,563-567.

[20] A. G. Fox and T. Li, Bell Sys. Tech. J. **40**, 453 (1961).

[21] S. Schneider, P. Borri, W. Langbein, U. Woggon, R. L. Sellin, D. Ouyang, and D. Bimberg, IEEE J. Quantum Electron. **40**, 1423 (2004).

[22] E. M. Purcell, Phys. Rev. **69**, 681 (1946).